Miniature Piezomotors

Resonant, Regenerative Switching Piezomotor Drive Amplifier

October 9, 2000

Wayne M. Zavis
Wilcoxon Research, Inc.
Gaithersburg, MD 20878

Sponsored by
Defense Advanced Research Projects Agency (DOD)
(Controlling DARPA Office)
ARPA Order D611/69

Issued by
U.S. Army Aviation and Missile Command
Contract Number: DAAH01-00-C-R040
Log Number: 99SB2-0194-1
DSO Topic: SB992-037-00

UNCLASSIFIED

DISTRIBUTION STATEMENT A
Approved for Public Release
Distribution Unlimited

20001013 030

Title:	Miniature Piezomotors
Subtitle:	Resonant, Regenerative Switching Piezomotor Drive Amplifier
Report Type:	Final Technical Report
Period Covered:	January 1, 2000 to June 30, 2000
Effective Date of Contract:	October 28, 1999
Contract Expiration Date:	June 30, 2000
SBIR Contract:	DAAH01-00-C-R040
Log Number:	99SB2-0194-1
DSO Topic:	SB992-037-00
Prepared By:	Wilcoxon Research, Inc. Gaithersburg, MD 20878 Wayne M. Zavis, Principal Investigator Wayne E. Shanks
Contributors:	Pennsylvania State University (PSU) Center for Acoustics and Vibration University Park, PA 16802 Jeremy Frank University of California at Los Angeles (UCLA) Active Materials Laboratory Los Angeles, CA 90095 Greg Carmen
Security:	Unclassified

REPORT DOCUMENTATION PAGE

Form Approved
OMB No. 0704-0188

Public reporting burden for this collection of information is estimated to average 1 hour per response, including the time for reviewing instructions, searching existing data sources, gathering and maintaining the data needed, and completing and reviewing the collection of information. Send comments regarding this burden estimate or any other aspect of this collection of information, including suggestions for reducing this burden, to Washington Headquarters Services, Directorate for Information Operations and Reports, 1215 Jefferson Davis Highway, Suite 1204, Arlington, VA 22202-4302, and to the Office of Management and Budget, Paperwork Reduction Project (0704-0188), Washington, DC 20503.

1. AGENCY USE ONLY (Leave blank)	2. REPORT DATE	3. REPORT TYPE AND DATES COVERED
	October 9, 2000	Final Technical Report (1/1/00 - 6/30/00)

4. TITLE AND SUBTITLE
Miniature Piezomotors,
"Resonant, Regenerative Switching
Piezomotor Drive Amplifier"

5. FUNDING NUMBERS
C: DAAH01-00-C-R040

6. AUTHOR(S)
Wayne M. Zavis & Wayne E. Shanks of Wilcoxon Research, Inc.
Jeremy Frank of Pennsylvania State University (PSU),
Greg Carmen of University of California at Los Angeles (UCLA)

7. PERFORMING ORGANIZATION NAME(S) AND ADDRESS(ES)
Wilcoxon Research, Inc., Gaithersburg, MD 20878
PSU, Center for Acoustics and Vibration, University Park, PA 16802
UCLA, Active Materials Laboratory, Los Angeles, CA 90095

8. PERFORMING ORGANIZATION REPORT NUMBER

9. SPONSORING/MONITORING AGENCY NAME(S) AND ADDRESS(ES)
Defense Advanced Research Projects Agency (DOD)
DSO, 3701 North Fairfax Drive, Arlington, VA 22203-1714
U.S. Army Aviation and Missile Command,
Bldg 7804, Room 205, Redstone Arsenal, AL 35898

10. SPONSORING/MONITORING AGENCY REPORT NUMBER
ARPA Order D611/69

Log No. 99SB2-0194-1

11. SUPPLEMENTARY NOTES
none

12a. DISTRIBUTION/AVAILABILITY STATEMENT
Approved for government agency release

12b. DISTRIBUTION CODE

13. ABSTRACT *(Maximum 200 words)*

Piezoelectric actuators and motors promise to deliver useful work at power densities an order of magnitude greater than that of their electromagnetic counterparts. The circuit concept developed is for a resonant, regenerative switching piezomotor drive amplifier that would efficiently transfer electrical energy that could be coupled into mechanical work through a piezoelectric actuator. The motor/amplifier system would operate at both electrical and mechanical resonances for the system. The amplifier's efficiency is estimated to be greater than 80% when driving a 1uF piezoelectric load with a 500 Vpk-pk signal. The available output power should be greater than 20 watts continuously from DC to 2.0 kHz. A prototype amplifier with +50% power efficiency is presently undergoing design debug and testing. Once operational, future amplifier refinements can focus on improved analog computation methodologies, mitigation of alignment and calibration difficulties, while trying to reduce sensitivity to actuator capacitance and improvements to output waveshape fidelity. Concurrently, a limited amount of effort was made towards miniaturization and optimization of two existing piezomotors. Improved models and experimental data will help enhance the future design of these prototype piezomotors.

14. SUBJECT TERMS
"resonant, regenerative piezomotor drive amplifier", piezomotor,
"piezoelectric power amplifier"

15. NUMBER OF PAGES
24

16. PRICE CODE

17. SECURITY CLASSIFICATION OF REPORT	18. SECURITY CLASSIFICATION OF THIS PAGE	19. SECURITY CLASSIFICATION OF ABSTRACT	20. LIMITATION OF ABSTRACT
Unclassified	Unclassified	Unclassified	

Table of Contents

List of Figures and Tables

1. Summary

The primary technical objective for Phase I research on this SBIR project was to develop generalized piezomotor drive electronics that efficiently operate at both electrical and mechanical resonance. This concept is called a Resonant, Regenerative Switching Piezomotor Drive Amplifier (R2amp). Concurrent with the electronic development activities, a limited amount of mechanical engineering effort was focused on miniaturization and optimization of existing piezomotors. Wilcoxon Research (WR) provided the lead on all electronic activities, while Pennsylvania State University (PSU) and the University of California at Los Angeles (UCLA) addressed issues associated with their specific piezomotor prototype implementations.

A final piezomotor drive amplifier circuit topology was defined for interfacing to PSU's resonant, roller-wedge piezomotor. The detailed design of each functional subsystem of the amplifier has been completed along with interconnect and packaging for the system. Construction of a proof-of-principle brass-board has been completed, as well as the testing of basic module performance. The proper operation of the high voltage and high power output drive section has proven to be elusive.

The performance expected from this proof-of-concept R2amp prototype had been estimated to be:

Drive capability:	1uF at 175 Vrms (500 Vpk-pk) at 80% efficiency
Output power:	20 watts continuous from DC to 2.0 kHz

Two technical issues prevented us from fully achieving these goals. First, the lack of one critical component, a high-voltage low-resistance MOSFET, prevented us from fully achieving these goals. Although promised by at least one semiconductor vendor during the period of performance of this contract, samples were never received. The most recent indications are that suitable parts will be available during Q4, 2000. The substitute parts would achieve 50 percent power efficiency rather than the 80+ percent expected.

Secondly, subtle timing issues in the signal paths of our "brass-board" R2amp prototype accounted for significant departure of designed versus implemented performance. In particular, to allow quick prototyping, the brass-board was laid-out without producing an optimized PC Board design. Unfortunately, it can be said that the "devil is in the details" and we have found that timing mismatches due to less than optimal board design has precluded a fully operational unit without creating a completely optimized layout. Through our Phase 1 effort, we have, however, gained valuable insight into the requirements needed to equalize the timing delays such that the performance of future circuits will be greatly enhanced.

We remain confident that the technical approach described in this report is viable. This confidence is borne out by both our modeling of the circuit performance and

the demonstration of the results presented in the remainder of this report. Our confidence in the technical feasibility is attested by a corporate investment of an additional $60k of effort beyond the allocated program budget to verify (1) that the concept is viable and (2) that it will ultimately result in successful realization of all technical objectives. In addition, we are also convinced that the technology created under this SBIR contract has significant commercial potential. To protect the intellectual property, we have filed a provisional patent on the unique amplifier drive circuitry.

Thus, in light of the issues highlighted, we feel that the concept has been proven to be viable. To complete the project, further support in Phase II is required as outlined below:

Phase 2 R2Amp, Year 1

Task	Task Description	Deliverables
1	Update current state-of-art benchmarks & technology	A.) Analysis report (vendors, technology, efficiency, price, etc.)
2	Define general application requirements and operating parameters (Voltage, current, bandwidth, distortion, efficiency, size, etc.)	B.) Requirements Specification C.) Test Specification and Requirements
3	Define implementation architecture	D.) Function block diagram
4	Functionally partition, model, simulate and analyze design (sub-modules and test requirements)	E.) Sub-module simulation reports
5	Schematic capture and component technology identification and selection	F.) Detailed schematic
6	Complete electrical simulation with updated sub-modules, simulations and analysis using wideband stripline techniques	G.) System simulation and report
7	Conceptualize packaging design (Thermal, EMC, voltage, mounting, etc.)	H.) Mechanical packaging concept and thermal model

8	Breadboard and test sub-module circuits (two iterations each)	I.) Functional sub-modules
9	Update electrical and packaging models and simulations	J.) Critical design review

Phase 2 R2Amp, Year 2

Task	Task Description	Deliverables
10	Design and construct ALPHA prototypes (four each)	K.) ALPHA PCB L.) ALPHA package M.) ALPHA test plan
11	Test and evaluate ALPHA prototypes	N.) Electrical test results and report O.) Environmental test results and report P.) Reliability/MTBF analysis report
12	Implement design changes from ALPHA prototypes	Q.) Updated BETA test plan
13	Design and construct BETA prototypes (four each)	R.) BETA PCB S.) BETA package
14	Test and evaluate BETA prototypes at a customer's site	T.) Electrical test results and report U.) Environmental test results and report
15	Analysis, conclusions and recommendations from BETA testing	V.) Final Report

2. Introduction

Piezoelectric actuators promise to deliver useful work at a power density an order of magnitude greater than that of electromagnetic motors and actuators. Even though the piezoelectric actuators have received much attention in the research community, little research has gone into the power systems needed to drive them. The purpose of this SBIR funded research was to develop a system where electrical energy could be efficiently coupled into mechanical work through a piezoelectric actuator.

Piezoelectric actuators differ from electromagnetic actuators in the load they present and mode by which they do work. Piezo-actuators produce very large forces, but over micron displacements. Useful work can only be extracted by accumulating the small stroke of the actuator at high frequencies. Since the actuator displacements are small and at high frequencies, the inertia and compliance of the mechanical accumulator must be taken into consideration. On every stroke of the actuator, energy is delivered to the mechanical load and deposited in the spring-like compliance of the actuator. The system's mass and compliance forms a mechanical resonant system, and energy not delivered to load will be lost to heat in the actuator structure. Thus, we can speak about the mechanical impedance of the actuator and load system. The portion of the load that does useful work has real impedance, and the portion of the load that stored energy in compression and momentum has an imaginary impedance. By driving the system at its natural mechanical resonance, the imaginary component of the mechanical impedance is canceled, leaving just the real component that does useful work.

Piezo-actuators also present a very large capacitive load. The first order electrical model for a piezo-actuator is a capacitor in series with a resistor. The resistor in the model represents the work-producing part of the mechanical load. Like the mechanical system, we can resonate the load capacitance to leave just the real part of the load. The problem is that practical considerations often (1) prevent the coincidence of electrical and mechanical resonances and (2) dictate that the actuator be driven over a wide band of frequencies. The actuator driver developed during this Phase I SBIR effort is able to drive just the real work-producing part of the system load over a broad range of frequencies from DC to several kHz, dramatically increasing the system power efficiency and full power bandwidth.

This SBIR contract made possible the development of a method for efficiently driving high-capacitive loads, at high power levels, with wide bandwidth waveforms. The resonant, switching regenerative piezomotor drive amplifier described here will not only drive high voltage piezoelectric actuators, but will also serve equally well in any application that requires high power drive signals to be applied to a predominantly capacitive load.

3. Background and Assumptions

The Resonant Regenerative Switching Amplifier (R2amp) combines the wide bandwidth and flexibility of a linear power amplifier with the high efficiency of a driven tank circuit. In a linear amplifier, high current is repeatedly sourced and then sunk when driving a capacitive load. On each cycle, the capacitor is loaded with energy and then this energy is discarded. At low to moderate frequencies, this wasted reactive power can be substantially larger than the power delivered to the work-producing part of the load, thus causing very low system energy efficiency (see Figure 1).

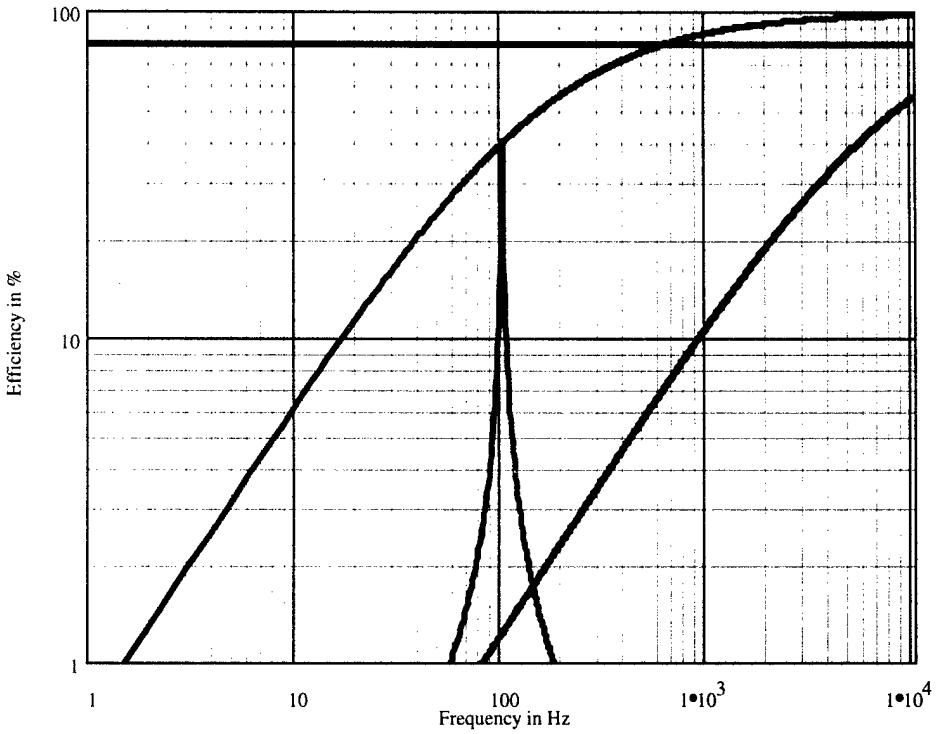

Black = Switching Regenerative Amplifier
Blue = Highest Efficiency of a Driven Tank Circui
Purple = Fixed Value Tank Circuit
Red = Linear Amplifier

Figure 1: Efficiencies for Piezo-Driver Systems

The wasteful reactive component of the impedance can be canceled by adding a conjugate inductance, leaving the load a pure resistance. Electrically this only occurs at one frequency, the resonant frequency of the LRC (tank) system. The

efficiency of this tank circuit can be explained by realizing that the energy stored on the capacitor is not thrown away, but transferred to the inductor and then transferred back to the capacitor every cycle. External power need only provide what is lost to mechanical work and resistive heating. The most efficient conversion of electrical energy to mechanical work will thus occur only at the narrow band of frequencies around electrical resonance. To make available a larger band of frequencies, the inductor value must be dynamically adjusted to change the resonant frequency. Since dynamically adjustable power inductors are currently impractical, the high-efficiency operation of the system is severely band limited. This problem of narrow-band operation can be overcome if the temporary energy storage is accomplished not in the inductor, but another capacitor. Analogous to water tanks, energy can be resonantly transferred between two capacitors, the load crystal and a storage capacitor, without dissipating appreciable power. Unlike energy stored in an inductor, the back and forth transfer of energy in the two capacitors can stop for an arbitrary period and then resume with little loss of energy. By transferring small bursts of energy at high frequencies, the voltage on the piezoelectric crystal can be ramped up or down in a piece-wise approximate to any arbitrary waveform. With this technique, the driver can operate with high efficiency at frequencies from DC all the way to some limiting frequency below the energy-transfer resonance. Present switching technology puts this upper frequency limit at several kHz, but tradeoffs in signal distortion and power efficiency can raise or lower this upper bound. A high level, conceptual schematic for such a system is presented in Figure 2.

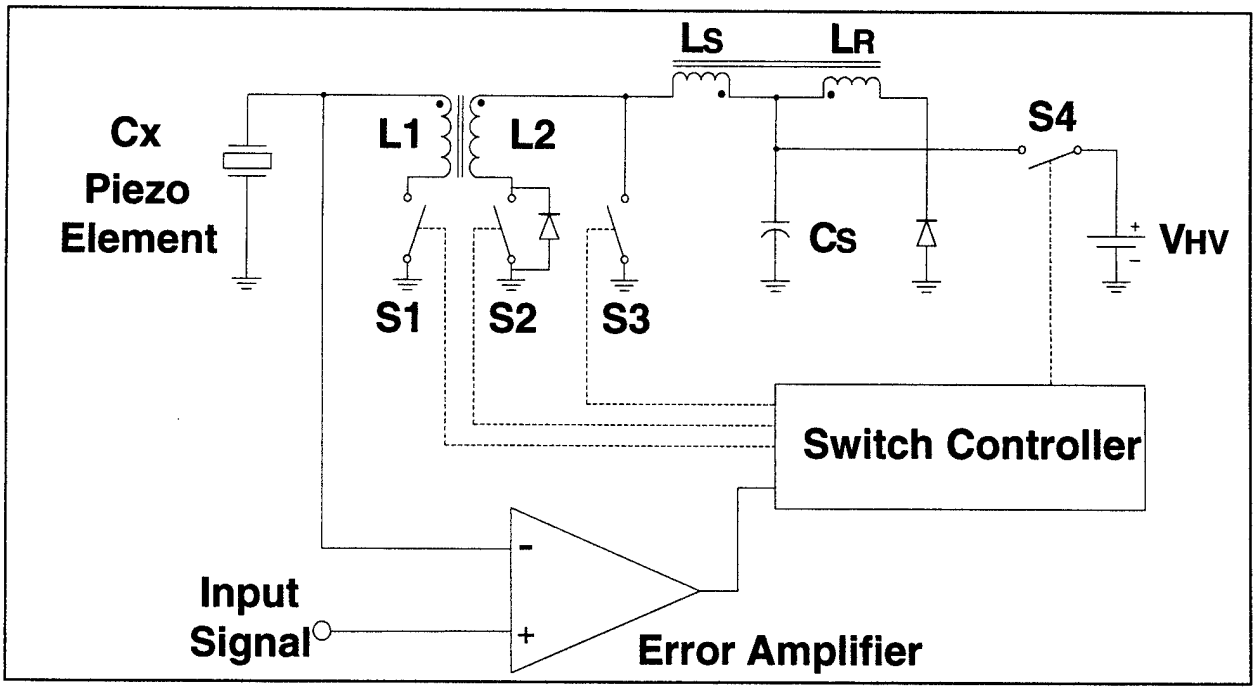

Figure 2: Regenerative switching piezomotor drive amplifier concept

4. Discussion and Results

4.1. Electronic Amplifier

Energy Transfer: The process of moving stored energy from one capacitor (Cx or Cs) to the other (Cs or Cx) is described here. For the purposes of this description, consider that the storage capacitor Cs starts out charged to the system's maximum potential (Vmax) and the piezoelectric element's capacitance Cx is at a 0 volts potential. All potentials are always positive, and Cs and Cx are equal valued capacitors. The circuit is designed to piece-wise approximate on Cx an arbitrary waveform seen at the error amplifier's input (VIN). At time zero, both the voltage on Cx (Vcx) and the input signal start at 0V.

The operation of this switching system can be put in two categories, (1) the transfer of energy from Cs to Cx (See Figure 3: Energy transfer timing diagram), and, (2) the transfer from Cx to Cs. The first of these two switching sequences, Cs to Cx, increases the voltage on the piezoelectric element (Vcx). This is initiated by the error amplifier when (VIN - Vcx) > $\alpha\Delta V$, where ΔV is voltage step size, and α is a constant ($0<\alpha<1$). When this condition is met, a current pre-load sequence is started in the switching controller by closing SW3. The need for a current pre-load before the actual energy transfer becomes apparent when we realize that during the transfer from Cs to Cx the system is a freely oscillating LC system with a positive slope on Vcx and an instantaneous current present in Ls. Since these boundary conditions of voltage and current are not present in the system during its hold state, where all the energy is sitting static on one of the two capacitors, for a given Vcx we must transfer some portion of the energy in Cs into Ls. The initial conditions needed to transfer energy into Cx are met when

$$\sqrt{V_{SS}^2 + V_X^2} - V_X \geq V_S$$

In the equation above Vss is the voltage on Cs before SW3 is closed, Vx is the voltage on Cx, and Vs is the dropping voltage on Cs. When the boundary conditions are met, the transfer of energy is started by opening SW3 and closing SW1 and SW2. L1 and L2 transformer couple Cx into Cs through Ls to form a freely oscillating LC system. Assuming there is sufficient energy contained in Cs for the transfer, Vcx increases until (Vcx - VIN) > (1 - α)ΔV. The transfer is terminated by the opening of SW1 and SW2. For most steps there will be some energy remaining in inductor Ls at the termination of the transfer. This energy is recovered through a diode connected between LR and ground. Most of the time this diode is reverse biased, thus preventing Cs from discharging through LR. During the inductor energy recovery phase, the collapsing field in the common core of Ls and LR forward biases the diode and current flows into Cs, thus recovering nearly all the

unused energy.[1] The system now enters a hold phase until the next transfer event starts.

The other possible switching event is the transfer of energy from Cx to Cs. This is initiated by the error amplifier when $(V_{CX} - V_{IN}) > \alpha\Delta V$. When this condition is met SW1 is closed and Cx starts to discharge through L1. If the potential on Cs permits, the body diode on SW2 is forward biased, thus Cx and Cs are transformer coupled through Ls. The transfer proceeds until $(V_{IN} - V_{CX}) > (1 - \alpha)\Delta V$, at which point SW1 is opened. If Vcs was too large to allow the diode on SW2 to forward bias when SW1 is closed, then the rapidly collapsing field in the core of L2, when SW1 is opened will forward bias the diode, and the energy will be transferred into Cs.

As described, energy can be efficiently transferred either into or out of Cx. New low on-resistance FET switches ensure that very little energy is lost to heat. With a slight addition in circuit complexity the diodes described above can be replaced with FET synchronous rectifiers. These FET switches behave like ideal diodes, and thus they dissipate very little energy when they conduct current. The circuit losses may be low, but they are non-zero. In addition, the piezoelectric element is dissipating energy in the form of mechanical work. At some point energy must be added to the system. This is accomplished by periodically charging Cs to a voltage that corresponds to the largest possible energy transfer from Cs to Cx. For a system with an energy step at the top of the voltage range, from 475V to 500V, the storage capacitor needs roughly 160V. If the Cs is ever below this potential, it is quickly charged to slightly greater then 160V, thus we are always guaranteed enough energy to make 25V steps all the way up to 500V. Since 160V represents the energy increment needed for one ΔV of 25V at around 500V, we expect that the maximum voltage on Cs to be 525V.

[1] The term "nearly all" is used since there will be a 0.7V forward-voltage drop in the diode. This voltage, times the current through the diode, will constitute a loss that results in heating of the diode.

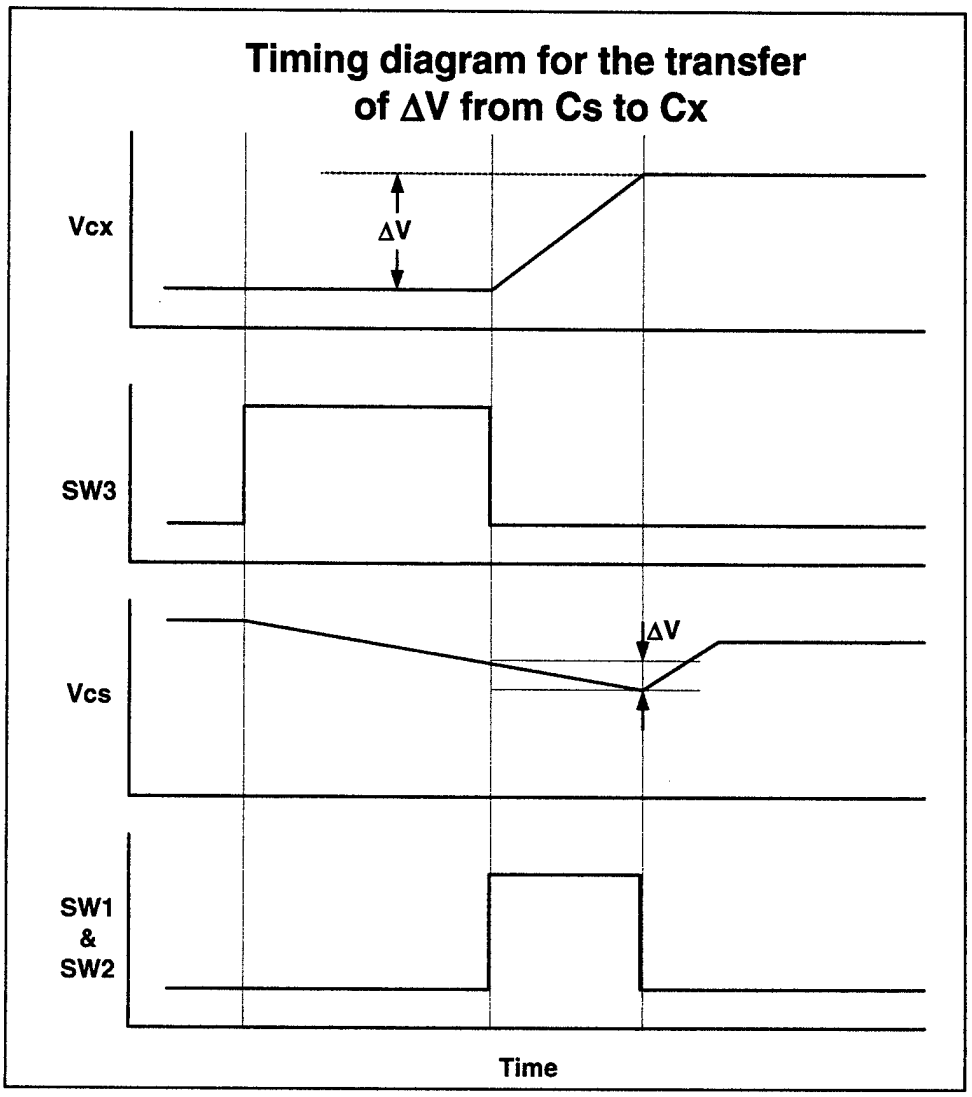

Figure 3: Energy transfer timing diagram

Design Results: Outlined above is the basic operation of the final drive amplifier. During the initial research portion of this project, several topologies were considered such as a switched quarter-wave transmission line, and an N-stage voltage swap topology. Although workable, these circuits were not chosen because of the difficulties in a practical circuit implementation. Figure 4 shows the circuitry for the actual power handling system used in the final resonant, regenerative switching piezomotor drive amplifier. Great effort was put into minimizing all power losses while dealing with the shortcomings of available circuit components. The enabling technology for this design implementation is the use of high voltage, high speed, N channel MOSFETs.

The system operates by chopping portions of the undriven LC resonance into discrete voltage steps at the actuator. The energy losses in the circuit come from resistive heating of the FET switches and other passive components. The FETs used have an on resistance of 0.2 ohms and dominate the losses of the system.

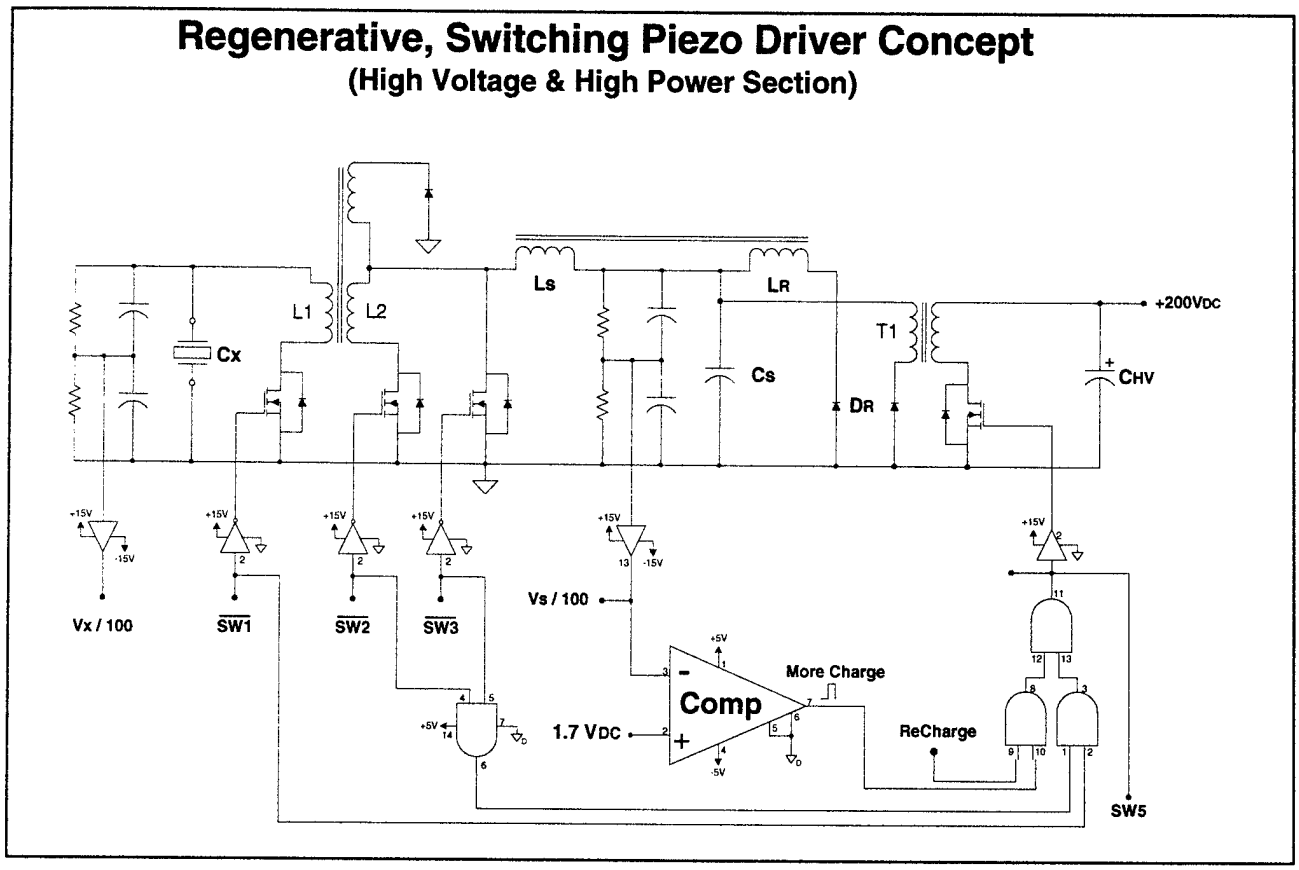

Figure 4: High voltage and high power output section

Total system equivalent resistance is of the order of one ohm. Therefore, most of the energy moving around within the system is delivered to the load with a real load resistance as low as 10 ohms. A second key feature of the chosen circuit topology is the exclusive use of ground referenced N channel MOSFETs. This feature greatly simplifies the circuit operation. None of the control voltages needs to be floated at high voltage. Highly efficient "over the counter" gate driver ICs are use that keep the switching transition time below 200ns. It should be noted that several methods for resonant piezoelectric drivers are patented (US 5,126,589, US 4,109,174, and US 4,767,959), but they are impractical because of difficulties associated with floating drive signals, inefficient diodes, BJT transistors, or SCRs. Diodes, BJT, and SCRs have a minimum forward voltage across their semiconductor junctions, thus they represent large V*I power losses. Our circuit implementation eliminated all such losses by using FETs that behave as ultra-small resistors when activated.

It should be noted that a few diodes have been used in this prototype power circuit. These diodes are used for simplicity in the proof of principle, but they would ultimately be replaced with FET switches that would act as synchronous rectifiers. Although it will be difficult to miniaturize this system down to the proposed 10 cubic centimeters using available discrete semiconductor components, the system is

easily several times smaller and lighter than a linear power supply capable of driving the same loads.

Prototype & Construction Limitations: The circuitry necessary to test and evaluate the performance of the proposed drive amplifier system was designed and built during Phase I. Six independent modules were designed and built:

1. High–power regenerative output drivers,
2. Regenerative driver switching controller,
3. Synchronized input power replenisher,
4. Speed normalized, energy step-size scaling,
5. PSU motor speed feedback sensor and controller, and
6. AC/DC power supplies.

Figure 5 is a photograph of the resulting prototype unit. However, due to construction limitations that were not fully appreciated until we reached the testing phase of the program, it was not possible to get the high-voltage and high-current portions of the design operational. Issues preventing the proper operation of this sub-section are associated with prototype circuit construction techniques used for high-speed power switching and high-voltage signal sensing. Additional problems in the same section arose from inductor winding techniques using large-gauge wire and the leakage inductance.

One of the major difficulties in prototyping the R2amp power amplifier was dealing with fast, high voltage/current signals. The switching frequencies within the R2amp can be up to the MHz range, and the rising and falling edges of the high voltage pulses are on the order of 100 nanoseconds. For traditional low voltage/current circuits one would not worry about wave and transmission line effects at these frequencies, because any ripples, or ringing seen on the signal or ground line might be two orders of magnitude lower than the signal. The R2amp, on the other hand, must consider the signal propagation in the layout due to the need to operate the switching logic at low-voltage levels (~5V) while the output switches 100's of volts. Hence, the sense-signal for the high voltage must be obtained through a –40dB attenuator. Noise spikes on the ground line are small compared to the 100V output steps, but they are large in comparison to the output sense voltage. Since proper operation of this resonant energy transfer system requires that the voltage and timing of the sense signals reflect the high power system to better than 5%, the R2amp circuit cannot tolerate the invasive noise generated by the high power switching system. A proper design of the high power system will reflect the design philosophies of working at 100 MHz, which will include a custom circuit board design that takes into consideration transmission line and impedance matching effects. In other words, a custom, impedance-designed board is necessary to ultimately make the concept function properly – a brass-board with wire-wrap and soldered jumpers cannot meet the critical timing and noise immunity requirements. Once we have a high power section that is capable of quietly slewing at rates of 100V per microsecond, then work on miniaturization and the optimization of the system Q can be addressed.

The performance of this prototype concept is estimated to be:

Drive capability:	1uF at 175 Vrms (500 Vpk-pk)
Efficiency:	+50%
Bandwidth:	DC to 2.0 kHz
Output power:	+20 watts continuous
Packaging:	125 cubic in. (excluding AC/DC power source)

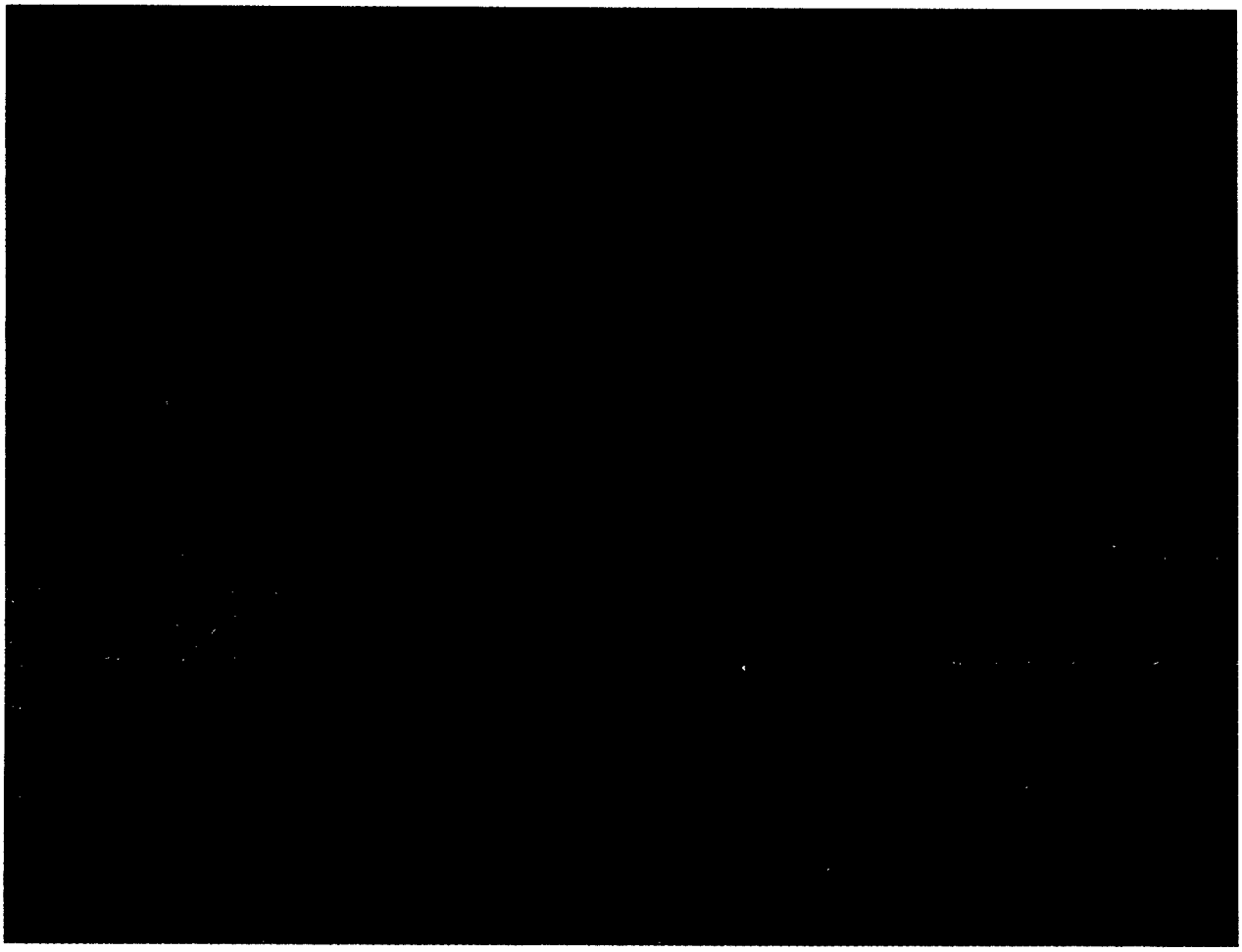

Figure 5: Prototype Piezo Amplifier

4.2. Resonant, Roller-Wedge Piezomotor

Piezomotor characteristics: PSU's Center for Acoustics & Vibration built and characterized the electro-mechanical performance of a prototype, 12-beam motor (See Figure 6) as follows:

Resonant Mode:	2nd at approximately 900 Hz
No-load Speed:	600 RPM (10 Hz)

Stall Torque:	0.5 N-m with the drive frequency increasing by approximately 10% at stall
Output Power:	4 Watts peak
Electric Drive:	130 Vac-pk (no DC offset) using standard linear drive electronics
Output Current:	220 mA-pk at peak power with 56 degrees of phase shift
Motor Efficiency:	46%

One of the 12 bimorph motor beam elements incorporates a strain sensing structure, which is used for resonance and feedback monitoring by the prototype amplifier. This sensing structure and dynamic control circuitry within the amplifier is necessary since the resonance of the piezomotor changes as a function of both rotational speed and output loading.

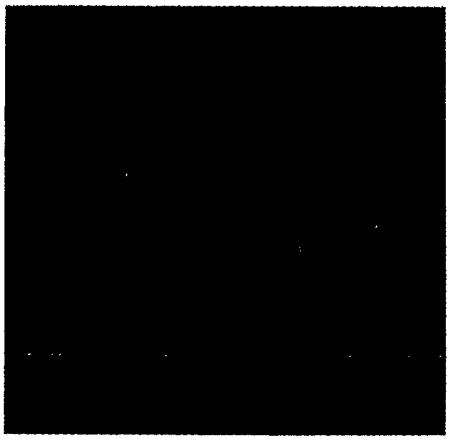

Figure 6: Roller-wedge piezomotor

Both no-load speed and stall torque increase linearly with drive voltage, when driven at resonance. The ceramic, bimorph beams can safely be driven up to 300 Vpk-pk (0.6 kV/mm, electric field break-down), which should therefore double both the no-load speed and stall torque, and quadruple the power output when driven at 300 volts.

Motor modeling: The rotary motor based on resonant bimorph beams was prototyped prior to the start of this project [1]. A subsequent series of prototypes with dimensional variations have been built since then. Tests were conducted on these prototypes in order to understand the operating mechanism as well as the output performance. Besides the virtues of low cost and simplicity of this novel design, the output energy density was measured up to 20 W/kg. Moreover, this

number could be further improved through a theoretical modeling and optimization process.

The effects of several variables such as reactive mass, hub mass, bimorph stiffness, and clutch design on the output performance have been tested and investigated. The operational principle is fully understood after a series of dynamic tests and measurements. It has been found that the motor will operate best when the bimorphs are driven at their second vibration mode. During this vibration mode, the reactive mass end of the bimorph remains almost unmoved, while the other end attached to the hub oscillates back and forth around the bearing's center. This movement is rectified by the roller clutch to constantly rotate the drive shaft in one direction.

Based on this experimental work, a piecewise linear mechanical model has been developed [2]. The simulation results from this linear, lumped component model shows good correlation with most of the experimental results, specifically that of output speed vs. output torque and driving frequency vs. output torque. Several observed trends from changing some design variables are also revealed by this model that will help to improve the overall design of the motor. However, some important characteristics of the motor can not predicted well by this simplified, linear model like clutch dynamics.

4.3. Piezoelectric Stacks

Setup & Procedure: Three commercially available, multilayer-glued piezoelectric stacks were tested. Dimensions and properties of these stacks are listed in Table 1. All stacks were coated with thin polymer to prevent dielectric breakdown and damage due to handling.

Table 1: Piezoelectric Stack Properties

Stack	Ax	Bx	Cx
Manufacturer	Physik Instrumente	Marco Inc.	NEC Corporation
Material	PZT	PZT	PZT
Actuator Area	5 mm x 5 mm	7.64 mm x 7.67 mm	5 mm x 5 mm
Actuator Heights	9 mm (A1) 18 mm (A2)	9 mm (B1) 18 mm (B2)	10 mm (C1) 20 mm (C2)
Active Regions	7.1 mm (A1) 16 mm (A2)	8.4 mm (B1) 17 mm (B2)	9 mm (C1) 18.5 mm (C2)
PZT layer thickness	100 μm	100 μm	110 μm
Capacitance	0.7 μF (A1) 1.8 μF (A2)	1.1 μF (B1) 2.2 μF (B2)	0.75 μF (C1) 1.45 μF (C2)
d_{33}	635 x 10^{-12} m/V (Bulk material)	700 x 10^{-12} m/V (Bulk material)	N/A
E_3	55 GPa (Bulk material)	N/A	44 GPa

Longitudinal strain (ε_{33}) as a function of stress (0 ~ 8 ksi) was measured using strain gages adhesively bonded on opposite faces of the stacks to monitor bending due to misalignment. The strain measurement was recorded using a high-speed, signal conditioning amplifier. These measurements were validated by comparing the results to data gathered with a LVDT (Linear Voltage Differential Transformer) for a zero load condition at 1 Hz. All data presented here is from the strain gage readings. During each test, four outputs were monitored including load applied from the test frame, current and voltage from the amplifier, and strain readings from strain gages. In addition to elastic modulus, strain as a function of electric field (0 ~ 2 MV/m) at 1 Hz and 10 Hz for various preloads (0 ~ 10 ksi) was measured. The strain readings were used to calculate piezoelectric constants for different compression loading conditions. Furthermore, effective permittivity as a function of electric field (0 ~ 2 MV/m) for various preloads (0 ~ 10 ksi) was also calculated. To eliminate nonlinear influence due to repeated tests, a strain reset procedure was applied prior to each test.

Mechanical & Electrical Properties: Young's modulus was measured at both open circuit condition (constant flux) and short circuit condition (constant electric field). In Figure 7, plots of strain versus stress for the short circuit (E = 0) and the open circuit (D = 0) are presented for stack A. The slope of each curve represents the Young's modulus (E_3). Approximate values for the Young's modulus are obtained by dividing the total strain ($\Delta\varepsilon$) by the total stress ($\Delta\sigma$).

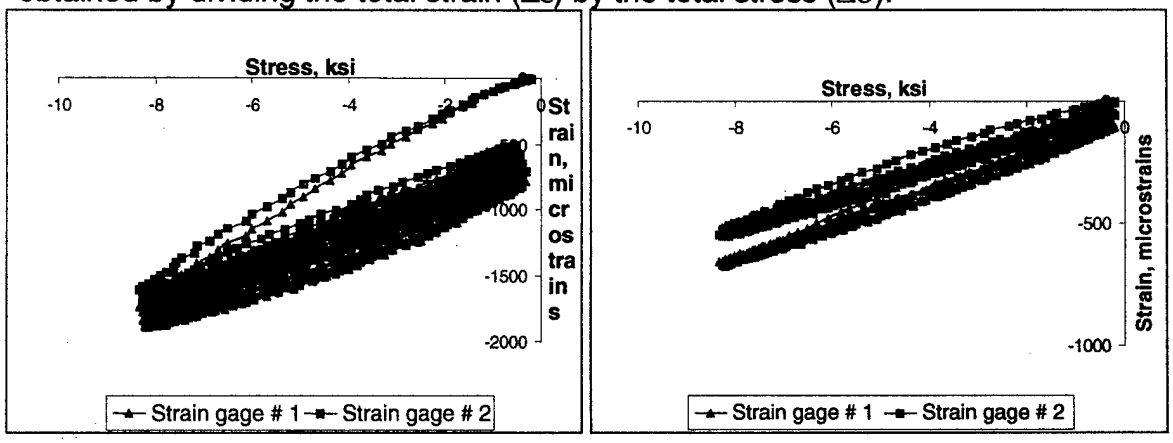

(a) Young's modulus at short circuit (Stack A) (b) Young's modulus at open circuit (Stack A)

Figure 7: Mechanical properties (measured at 1 Hz)

In Figure 8, the Young's modulus of all stacks for both electric conditions are presented. For the short circuit condition, strain readings from the two gages were all within 10% difference. However, strain readings from two gages for the open circuit condition were between 10% to 20%. These differences in Figure 8 were observed for all stacks.

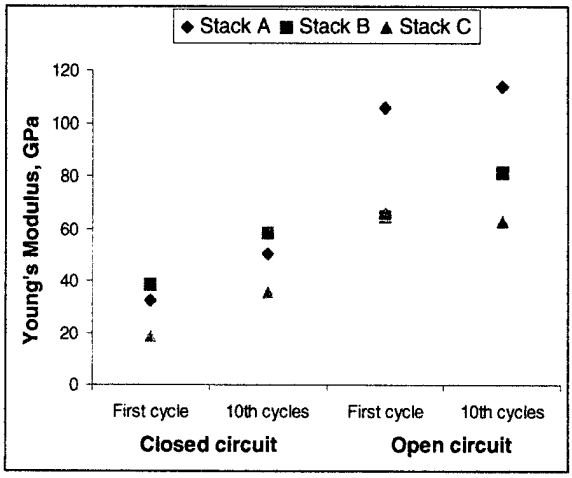

Figure 8: Young's modulus at different electric conditions (frequency at 1 Hz)

Strain output as a function of electric field for a wide range of mechanical preloads was evaluated. The tests were conducted under load control with a sinusoidal electric field varying between 0 to 2 MV/m. In Figure 9(a), strain output as a function of electric field for various constant applied preloads is presented for the stack A. Data presented here is for electrical loading at 1 Hz. All other stacks showed similar trends in the strain versus electric field curve. In Figure 9(b), the piezoelectric constant (d_{33}) versus mechanical preload for all the stacks is presented. The piezoelectric constant was calculated by dividing the total strain ($\Delta\varepsilon$) by the total electric field (ΔE). Strain measurements using strain gages were close to the measurements using LVDT (less than 3% difference), except for stack C which had a 14% difference. Therefore, two curves are presented for stack C, with the second curve having adjusted data values normalized to the measured LVDT data. As expected, there is an optimum mechanical preload to maximize the piezoelectric constant for each stack. Under the optimum preload, the piezoelectric constant increases up to 70% compared to one without preload. Generally, a mechanical preload increases strain output by rotating domains perpendicular to the preload direction, and those rotated domains realign parallel to the electric field when the electric field is applied. Consequently, a specific mechanical load allows maximum realignment of domain when a specific electric field is applied.

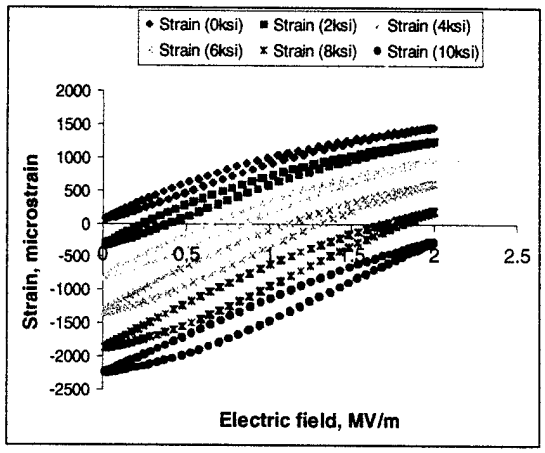

(a) Strain vs. Electric field with different preload (stack A @ 1 Hz)

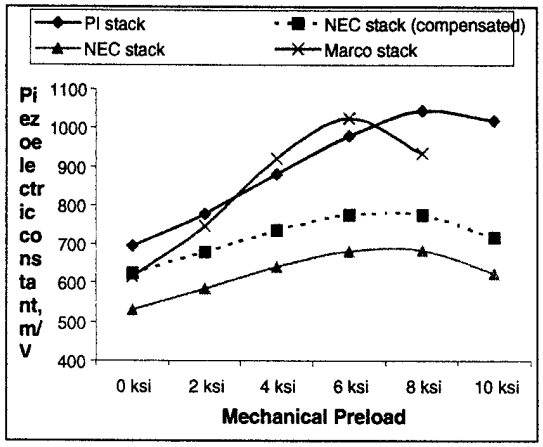

(b) Piezoelectric constant as a function of preloads

Figure 9: Mechanical displacements at different mechanical preloads

5. Conclusion

The primary technical objective for Phase I research on this SBIR project was to develop generalized piezomotor drive electronics that efficiently operate at both electrical and mechanical resonance. Concurrent with the electronic development activities, a limited amount of mechanical engineering effort was focused on miniaturization and optimization of existing piezomotors. Wilcoxon Research (WR) provided the lead on all electronic activities, while Pennsylvania State University (PSU) and the University of California at Los Angeles (UCLA) addressed issues associated with their specific piezomotor prototype implementations.

The power efficiency of the R2amp amplifier has been calculated to be greater than 80% when driving a 1uF piezoelectric load with a 500 Vpk-pk signal. The available output power should be greater than 20 watts continuously from DC to 2.0 kHz. A prototype amplifier with +50% power efficiency was designed, built, and underwent debug, and test. Much of this effort was funded by Wilcoxon Research with resources to augment that received from the SBIR contract.

Two technical issues prevented us from fully achieving our Phase 1 goals. First, the lack of one critical component, a high-voltage low-resistance MOSFET, prevented us from fully achieving a unit capable of attaining 80% efficiency. Secondly, subtle timing issues in the signal paths of our "brass-board" R2amp prototype accounted for significant departure of designed versus implemented performance. In particular, less than optimal board design precluded a fully operational unit. Through our Phase 1 effort, we have, however, gained valuable insight into the requirements needed to equalize the timing delays such that the performance of future circuits will be greatly enhanced.

Our conclusion is that the technical approach described in this report is viable. This confidence is borne out by both our modeling of the circuit performance and the demonstration of the results presented in this report. Our confidence in the technical feasibility is attested by a corporate investment of an additional $60k of effort beyond the allocated program budget to verify (1) that the concept is viable and (2) that it will ultimately result in successful realization of all technical objectives. In addition, we are also convinced that the technology created under this SBIR contract has significant commercial potential. To protect the intellectual property, we have filed a provisional patent on the unique amplifier drive circuitry.

Once operational and fully tested, future amplifier design generations can focus on improved analog computation methodologies (squares & square root calculations), mitigation of alignment and calibration difficulties, while trying to reduce sensitivity to actuator capacitance and improvements to output waveshape fidelity. Present technology is well suited for the scale-up of both the reactive and delivered power of the regenerative driver.

6. References

[1] Jeremy Frank, etc. "*Design and Performance of a Resonant Roller Wedge Actuator*", SPIE Proceedings of Smart Structures and Materials 2000, New Port Beach, CA

[2] Eric Mockensturm, etc. "*Modeling and Simulation of a Resonant Bimorph Actuator Drive*", Proceedings of ONR Piezoelectric Materials and Devices, Penn State University, 2000

7. Distribution List

Commander (2 Copies)
U.S. Army Aviation and Missile Command
ATTN: AMSAM-RD-WS-DP-SB (C. Tom Phillips, Tech Monitor)
Bldg 7804, Room 205
Redstone Arsenal, AL 35898

Commander (1 Copy)
U.S. Army Aviation and Missile Command
ATTN: AMSAM-RD-OB-R
Bldg 4484, Room 204
Redstone Arsenal, AL 35898-5241

Commander (1 Copy)
U.S. Army Aviation and Missile Command
ATTN: AMSAM-RD-WS
Bldg 7804, Room 247
Redstone Arsenal, AL 35898-5248

Director (1 Copy)
Defense Advanced Research Projects Agency
ATTN: DSO (Dr. Ephrahim Garcia)
3701 North Fairfax Drive
Arlington, VA 22203-1714

Director (1 Copy)
Defense Advanced Research Projects Agency
ATTN: ASBD/SBIR
3701 North Fairfax Drive
Arlington, VA 22203-1714

Director (1 Copy)
Defense Advanced Research Projects Agency
ATTN: ASBD/DARPA Library
3701 North Fairfax Drive
Arlington, VA 22203-1714

Defense Technical Information Center (2 Copies)
ATTN: Acquisitions/DTC-OCP, Rm-815
8725 John J. Kingman Rd., STE 0944
Ft. Belvoir, VA 22060-6218